TRENDS IN SCIENCES 2026; 23(10): 13258
https://doi.org/10.48048/tis.2026.13258 RESEARCH ARTICLE

# Bio-Coating from Chitosan-Zinc Oxide Nanocomposite for Storage Life Extension of Monthong Durians

**Paweena Porrawatkul[1,2,*], Prawit Nuengmatcha[2,3], Rungnapa Pimsen[1,2], Montakarn Thongsom[4], Arnannit Kuyyogsuy[1,2], Benjawan Ninwong[1,2] and Nichapa Rattanakomon[1]**

[1]*Department of Chemistry, Faculty of Science and Technology, Nakhon Si Thammarat Rajabhat University, Nakhon Si Thammarat 80280, Thailand*
[2]*Center of Excellence in Nanomaterials Chemistry, Faculty of Science and Technology, Nakhon Si Thammarat Rajabhat University, Nakhon Si Thammarat 80280, Thailand*
[3]*Creative Innovation in Science and Technology, Faculty of Science and Technology, Nakhon Si Thammarat 80280, Thailand*
[4]*Department of Biology, Faculty of Science and Technology, Nakhon Si Thammarat Rajabhat University, Nakhon Si Thammarat 80280, Thailand*

**([*]Corresponding author's e-mail: paweena_por@nstru.ac.th)**

*Received: 4 January 2026, Revised: 24 March 2026, Accepted: 5 April 2026, Published: 10 May 2026*

**Abstract**

Durian (*Durio zibethinus* Murray.) is a climacteric fruit prone to rapid postharvest ripening, limiting its storage life during long-distance transport. This study developed an edible bio-coating of chitosan-alginate incorporating green-synthesized zinc oxide nanoparticles (ZnO NPs; 30 ± 4.6 nm) from *Terminalia catappa* leaf extract (ZnO NPs/CS) to delay ripening and preserve the postharvest quality of Monthong durian. Effects on weight loss, total soluble sugar content, peel color (L*, a*, b*, and ΔE), and Zn residue were evaluated over 10 days of storage under ambient conditions. ZnO NPs/CS-coated durians showed significantly reduced weight loss (< 6.19 ± 0.39% at day 10 vs. 13.76 ± 0.79% in uncoated fruit). Total soluble sugars increased more slowly in coated fruit, reaching 21.67 ± 0.40 g/100 g at day 10 compared to 23.95 ± 0.27 g/100 g in uncoated samples. Color analysis indicated coated durians retained higher lightness (L*) and greenness (a*), with slower yellowness (b*) development and lower total color difference (ΔE), consistent with delayed ripening. Atomic absorption spectrometry confirmed no detectable Zn in edible pulp across treatments, with only trace levels (0.08 ± 0.002 mg/kg) in the inner peel of coated durians, indicating surface confinement of ZnO NPs. The ZnO NPs/CS coating acted as a semi-permeable barrier, mitigating moisture loss, sugar accumulation, and ripening-related changes while ensuring food safety. This sustainable approach extends durian storage life and marketability, with potential for other climacteric tropical fruits.

**Keywords:** Durian, Bio-coating, Zinc oxide nanoparticles, Chitosan, Postharvest quality, Ripening delay, Weight loss, Sugar accumulation, Food safety

## Introduction

Durian (*Durio zibethinus* Murray) is a tropical fruit widely grown in Southeast Asia and is known as the "king of fruits" because of its distinct, potent scent and its delicious, custard-like flesh. In Thailand, durian holds significant economic importance as a leading fruit export. The country supplies large volumes of durian to international markets, with primary destinations being Hong Kong, China, and Taiwan. Monthong durian is harvested at approximately 70% - 80% physiological maturity and requires about 8 - 9 days to naturally ripen after harvest [1]. Transporting durian through a long transport time should regard the condition of storage, such as temperature, minimum oxygen concentration and maximum carbon dioxide concentration [2]. Durian

is commonly transported in refrigerated containers with ventilation systems to manage the heat generated during respiration. To prevent quality deterioration, the container temperature is generally set below 20 °C, while 15% - 20% of ventilation rates are applied to expel internal heat before the fruit reaches end consumers [3].

The ripening and respiration processes are correlated to physiological and biochemical changes, resulting in changes in color, firmness and texture, starch conversion, and volatile production [4]. Sulfur-containing compounds and esters derivative compounds are produced during durian ripening. Durian starch is composed of amylose and amylopectin, with amylopectin constituting more than 90% [5]. Starch and sugars play critical roles in determining fruit quality and supporting fruit growth and development [6]. In long-distance transportation, especially by land, even small changes in temperature or relative humidity might cause excessive heat to build up due to metabolic processes [7]. This reasons the fruit to ripen too early, lose weight, become soft, and smell foul [8]. These effects get poorer quality when there is mechanical stress, including vibration, collision, or compression.

Fruit coating is another popular option because it produces a mechanical barrier that restricts gas exchange between the fruit and its surrounding atmosphere, creating a modified atmosphere with enhanced $CO_2$ and reduced $O_2$ levels [9]. In particular, an intriguing coating technique is bio-coating. Bio-coatings have become a convenient technique because they act as a semi-permeable barrier against oxygen, carbon dioxide, ethylene, and water vapor [10]. These coatings can inhibit ripening, block processes produced by ethylene, and keep the fruit's texture and taste the same while it is being shipped and stored for a long time [11]. Therefore, creating coatings with specific qualities is a beneficial way to address logistical challenges in durian exports and make the business more sustainable.

Most biodegradable coatings produced typically contain metal oxide nanomaterials as an ingredient due to their unique properties [12-14]. Metal oxides, such as magnesium oxide (MgO) [15], titanium dioxide ($TiO_2$) [16], and zinc oxide (ZnO) [17], have been reported to exhibit superior antibacterial activity and stability compared to organic antimicrobial agents. In comparison to other metal oxides, ZnO nanoparticles (ZnO NPs) are considered safe materials for human beings. ZnO NPs are safe to use. For example, ZnO NPs are used in the linings of meat, fish, corn and pea cans to preserve their color and prevent them from going bad [18]. Numerous studies proposed methods used to incorporate ZnO nanoparticles with gelatin [19], aloe gel [20], polypropylene [21] alginate [22] and chitosan [23]. Biopolymers are excellent carriers for active agents because they can be controlled and released in different ways [24,25]. They can also be mixed or assembled in layers to make a specific application. Chitosan is a biopolymer that is not harmful, forms films, and breaks down naturally. It also has antibacterial qualities, making it ideal for creating food packaging that combats germs [26].

Several research topics have been interested in bio-coating composites incorporating nanomaterials to extend fruit life. These coatings, which are edible and biocompatible, utilize nanoparticles, such as chitosan, ZnO, Ag, or nanoemulsions, to improve barrier properties, reduce respiration rates, and inhibit microbial growth [27]. Bio-coatings with metal nanoparticles like ZnO and Ag in nanocomposite films have been investigated for tropical fruits such as berries [28], apple [29], guavas [30], banana [31] mango [32] and tomato [33]. These effectively reduce weight loss, color changes, and spoilage. However, there is currently no research studying the development of bio-coating for Monthong durian to delay ripening, which would be good for export because it takes a long time to ship.

This study is the first to apply zinc oxide nanoparticles (ZnO NPs), synthesized via green chemistry and combined with chitosan biopolymer and alginate as a gelling agent as a bio-coating on Monthong durian fruit to delay ripening. It includes detailed structural and morphological characterization of the ZnO NPs and evaluates various ZnO NP-chitosan coating formulations. Moreover, the coatings demonstrated anti-*Phytophthora* activity and effectively delayed ripening, preserved the fruit quality, and extended the shelf life of Monthong durian.

## Materials and methods

### Materials

The Mon Thong durians were collected from Suan Rian Namjai, Bang Phan Subdistrict, Bang Khan District, Nakhon Si Thammarat Province, Thailand

(8.72802°N, 99.75285°E; WGS84). Selections were made based on equivalent weight, origin, and planting timeframe. Each treatment consisted of 3 biological replicates, with durian fruits of similar maturity and size randomly assigned to each treatment group. Storage experiments were conducted under ambient laboratory conditions at 32 ± 1.0 °C and 60% - 80% relative humidity (RH). Since all treatments were stored under identical conditions, any humidity variations affected all samples equally. All reagents used were analytical grade reagents, and DI water was used throughout the experiment. Chitosan, which has a high molecular weight of 31 - 37 kDa and deacetylation degree 75% was purchased from Sigma Aldrich Chemie GmbH. Ethanol absolute and zinc acetate dihydrate were acquired from Sigma-Aldrich (Steinheim, Germany). Glacial acetic acid and sodium hydroxide (NaOH) were purchased from Alfa Aesar (Kandel, Germany), while sodium alginate was obtained from PanReac (Barcelona, Spain). All microbiological reagents were purchased from Biokar (Allonne, Beauvais, France).

**Preparation of *Terminalia catappa* leaf extract**

Fresh leaf of *Terminalia catappa* (*T. catappa*) were collected from Nakhon Si Thammarat Rajabhat University, Nakhon Si Thammarat Province, Thailand. They washed with deionized water several times to remove residues. Cut into small pieces and dry at room temperature. Further, 10 g of dry leaf were added to a specific amount of DI water in a glass beaker, followed by boiling at 60 °C for 90 min with continuous stirring at 450 rpm, resulting in a reddish-yellow-colored solution. Then the leaf extraction solution was placed to cool down at room temperature. The extraction solution was filtered through No. 1 filter paper, after which the solvent was evaporated using a rotary evaporator. The crude extract of *T. catappa* leaf were obtained and stored at 4 °C in a laboratory refrigerator. The final extract was used as a reducing and stabilizing agent.

**Green synthesis of zinc oxide nanoparticles**

Zinc oxide nanoparticles were synthesized via a simple and fast co-precipitation method [34]. First, 10.2 g of Zn $(CH_3COO)_2 \cdot 2H_2O$ and different amounts (0.2, 0.5 and 0.8 g) of *T. catappa* leaf extract were dissolved in 40 mL of DI water under continuous stirring until a homogeneous mixture was obtained. Then the reaction of the solution was carried out under sound waves at 70 °C for 30, 60 and 90 min. Then, 2 M NaOH was used to adjust the pH of the solution to 10, which turned the initially transparent solution milky-white. Finally, the precipitate of ZnO NPs was washed several times with DI water and absolute ethanol to remove the remaining extract and dried in air at 60 °C for 24 h.

**Characterization techniques**

UV-Visible Diffuse reflectance spectrophotometry (Agilent, AL-SYS-UV-6000-M) was used to study the ZnO NPs absorption spectra in the 300 - 800 nm range. The morphology of the NPs was studied by scanning electron microscopy (SEM, Quanta 400) and transmission electron microscopy (TEM, JEOL-2010, JEM-2100 F, 100 kV). The elemental composition of the materials was investigated by energy-dispersive x-ray spectroscopy (EDX, Quanta 400).

The crystallinity of the NPs was evaluated by X-ray diffraction (XRD, Xpert-Pro, using Cu-Kα (1.54056 A) and 45 kV/40 mA). Furthermore, the particle size of the materials was determined using a laser particle size analyzer (LPSA, Beckman Coulter, LS 320).

**Preparation of bio-coatings**

The preparation of bio-coatings was adapted from Arroyo *et al.* [30]. Briefly, a 1.5% (w/v) sodium alginate (SA) solution was prepared in 100 mL of deionized (DI) water and sonicated with heating at 70 °C until clear (~3 h). Separately, 5 g of chitosan was dissolved in 300 mL of 1% (v/v) acetic acid by heating to 60 °C and stirring until fully dissolved. The SA and chitosan solutions were then combined and homogenized to form a uniform mixture, followed by the addition of 1 mL of 2% (v/v) glycerol solution and stirring for 6 - 10 min. ZnO NPs were subsequently incorporated at concentrations of 3% (w/w), 5% (w/w), 7% (w/w), 8% (w/w), or 9% (w/w). Durians were dipped once in the resulting ZnO NP-chitosan-alginate (ZnO NP-CS-SA) bio-coating for 5 min, after which the coating's efficacy in delaying ripening was evaluated. The schematic illustrating the green synthesis of ZnO NPs and the process for preparing bio-coatings is shown in **Figure 1**.

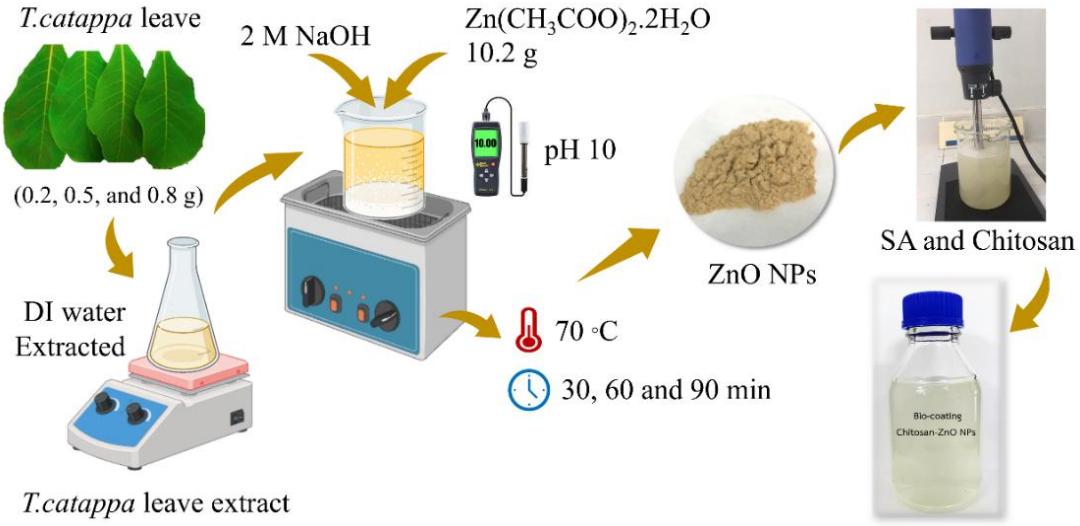


**Figure 1** Schematic diagram of the green synthesis of ZnO NPs using *Terminalia catappa* leaf extract as a reducing and stabilizing agent, alkaline precipitation with 2 M NaOH and zinc acetate dihydrate ($Zn(CH_3COO)_2 \cdot 2H_2O$), pH adjustment to 10, and thermal treatment at 70 °C for 30 - 90 min, followed by incorporation of ZnO NPs into sodium alginate (SA) and chitosan matrix for bio-coating preparation.

**Evaluation of antifungal (*Phytophthora spp.*) activity**

The antifungal activity of bio-coating of all samples that varied in ZnO NPs concentrations of 3% (w/w), 5% (w/w), 7% (w/w), 8% (w/w) and 9% (w/w) was screened by the agar diffusion method. Preparation of fungi of the *Phytophthora spp*. by cutting the hyphae of *Phytophthora spp*. using a cork borer and placing them on solid PDA medium and incubating at 35 °C for 5 days to allow the fungi to fully develop. After incubation, the diameter of inhibitory zones was measured in mm, and 3 replicates were verified for the activity of bio-coating samples against tested fungi.

**Determination of total sugar content**

Total sugar content of durian pulp was determined following the AOAC official method 925.35B (Lane-Eynon titration using copper reduction) [35]. Briefly, a known amount of durian pulp (10 g) was homogenized with distilled water and clarified using Crrez I and II reagents. The filtrate was hydrolyzed with 1 N HCl at 70 - 80 °C for 30 min to turn sucrose into reducing sugars. Then, it was neutralized with NaOH and filtered. The reducing sugars in the hydrolyzed solution were quantified by titration with Fehling's A and B solutions using methylene blue as an indicator. Total sugar content was calculated and expressed as grams of invert sugar per 100 g of sample (g/100g).

**Determination of durian peel color**

For determination of Monthong durian peel color using a UV-Visible Diffuse reflectance spectrophotometry (Agilent, AL-SYS-UV-6000-M). The color, expressed in the CIE Lab (L a b) system, is numerically specified in a 3-dimensional spherical space defined by the 3 perpendicular axes: the "L" axis (brightness) ranging from black (0%) to white (100%); the "a" axis, from green (−a) to red (+a); and the "b" axis, from blue (−b) to yellow (+b). Total color difference (ΔE) was calculated using L, a, and b values as per Eq. (1):

$$\Delta E^* = [\Delta L * 2 + \Delta a * 2 + \Delta b * 2]^{1/2} \quad (1)$$

where ΔL, Δa, and Δb represent the difference in L, a, b-values at a particular interval from the respective initial values.

**Determination of zinc residues**

After coating the durian with a bio-coating using chitosan and ZnO NPs, residues of the Zn element will be checked for coated durian pulp and inner skin of the durian peel by atomic absorption spectrophotometry

(AAS). Samples were prepared using wet digestion by baking at 100 °C to dry, then cutting and grinding finely. Then, it was weighed to approximately 1 g and digested in a beaker by adding 1 mL of concentrated nitric acid and left in a fume hood for 24 h to obtain a dark yellow solution. Then take the sample in a beaker and heat it to 80 °C while continuously stirring the solution until a clear, colorless solution is obtained. Then take the solution obtained after digestion. Filter into a 50 mL volumetric flask and adjust the volume with 0.01 M nitric acid ($HNO_3$) until 50 mL is complete. The obtained samples were analyzed for quantity.

### Statistical analysis

All data were expressed as mean ± SD ($n \geq 3$). Statistical differences among treatments were analyzed by one-way ANOVA followed by Tukey's HSD test at $p < 0.05$. All analyses were performed using SPSS software version 26.0 (IBM Corp., Armonk, NY, USA). Although formal tests of normality and homogeneity of variance were not performed, experimental data showed comparable variance among treatments, and ANOVA is generally strong to moderate deviations from these assumptions. Therefore, the applied statistical approach remains appropriate for comparative analysis.

## Results and discussion

### Synthesis of ZnO NPs

UV-Visible absorption spectra in **Figure 2(a)** exhibit the ZnO NPs synthesized with varying quantities of *T. catappa* leaf extract (0.2, 0.5 and 0.8 g). All samples show a different absorption peak in the UV region (around 370 - 400 nm), corresponding to the band gap absorption of ZnO NPs [36]. The absorbance intensity increased with leaf extract concentration up to 0.5 g, indicating that an optimal quantity of biomolecules from the extract acted as both reducing and stabilizing agents to promote ZnO NP nucleation. However, further increasing the extract amount to 0.8 g reduced the absorbance intensity, likely due to excessive organic compounds causing particle agglomeration or decreased crystallinity. Therefore, 0.5 g of *T. catappa* leaf extract appears to be the most suitable concentration for the efficient synthesis of ZnO NPs. **Figure 2(b)** illustrates the effect of sonication time (30, 60 and 90 min) on the UV-Vis spectra of the synthesized ZnO NPs. The samples that were sonicated for 60 min had the highest absorbance. This means that the particles were smaller and better dispersed since the ultrasonication created a strong cavitation effect [37]. While a sonication time of 30 min may not provide appropriate energy for complete nucleation, a prolonged sonication time of 90 min could cause particle agglomeration or surface defects, resulting in a slight decrease in absorbance intensity [38]. The variation in both extract amount and sonication time significantly affects the optical properties and creation efficiency of the biosynthesized ZnO NPs. The optimal synthesis condition was created to be 0.5 g of *T. catappa* leaf extract and 60 min of ultrasonication, yielding ZnO NPs with strong UV absorption, indicating high purity and uniform particles distribution. This showed that the particles were very pure and evenly distributed. Plant extracts are used in the biosynthesis process.

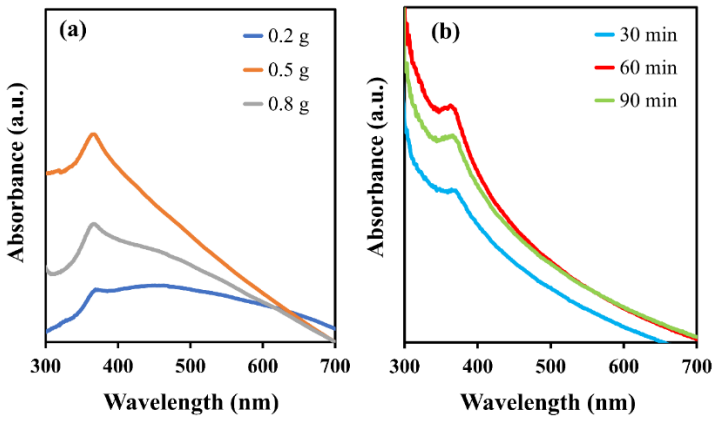


**Figure 2** UV-Visible spectrum of optimization of green synthesized ZnO NPs; (a) optimization of *T. catappa* leaf extract (0.2, 0.5 and 0.8 g) and (b) optimization of sonication time (30, 60 and 90 min).

**Characterization of ZnO NPs**

**SEM and EDX analysis**

**Figure 3(a)** presented the surface morphology of ZnO NPs synthesized using *T. catappa* leaf extract as a reducing and stabilizing agent. The SEM image reveals a condensed aggregation of nanosized particles with mainly quasi-spherical and hexagonal morphologies [39]. The formation of these nanoscale sample aggregates proposes successful nucleation and growth of ZnO crystals is facilitated by main phytochemicals such as phenolics, flavonoids, and tannins present in *T. catappa* leaf extract [40].

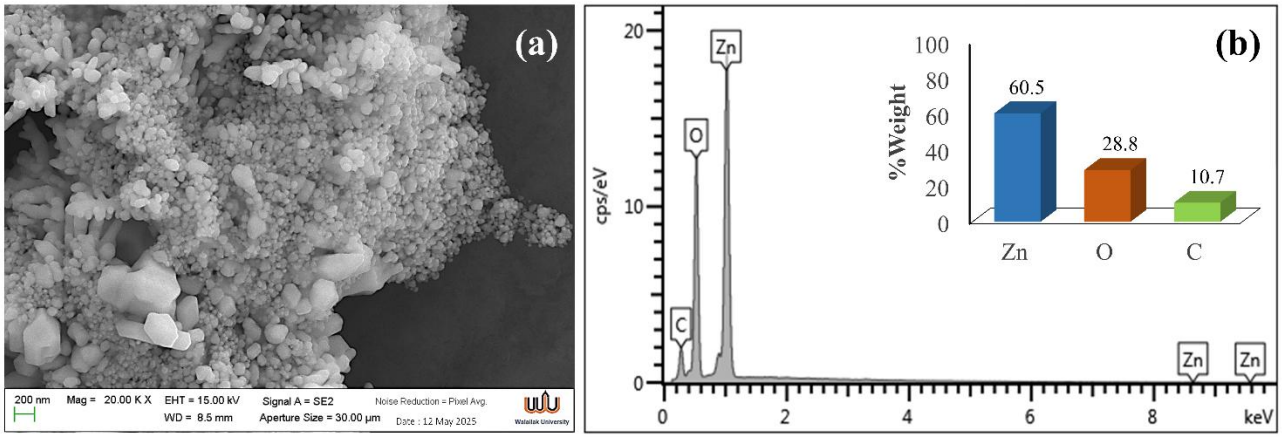


**Figure 3** Morphological and elemental characterization of ZnO NPs synthesized using *Terminalia catappa* leaf extract; (a) SEM image of green synthesized of ZnO NPs and (b) EDX spectrum and %wt of element composition of green synthesized of ZnO NPs.

**Figure 3(b)** showed the corresponding EDX spectrum confirming the elemental composition of the green synthesized ZnO NPs. Strong characteristic peaks at approximately 1.0 and 8.6 keV correspond to Zn Kα and Zn Kβ lines, respectively, verifying the presence of zinc as a major component. A noticeable oxygen peak around 0.5 keV indicates the formation of Zn-O bonds, confirming the successful synthesis of ZnO NPs. There is also a weak carbon element peak, which is a signal of organic residues of *T. catappa* leaf extract that have been trapped to the surface of the nanoparticle [41]. The insert bar graph demonstrated the quantitative composition, showing 60.5 %wt of Zn, 28.8 %wt of O, and 10.7 %wt of C. The Zn:O ratio close to stoichiometric ZnO further supports the formation of pure zinc oxide with slight carbon incorporation from the natural reducing agents [42]. SEM-EDX analysis revealed that the *T. catappa* leaf extract-mediated synthesis yielded well-crystallized ZnO NPs with homogeneous elemental distribution, confirming the efficacy of this green method as an eco-friendly alternative to conventional chemical approaches.

**TEM analysis**

The morphology and microstructure of green-synthesized ZnO NPs were characterized by transmission electron microscopy (TEM), as shown in **Figure 4(a)**. The TEM image revealed a plate-like morphological structure in nanometer range. High-resolution TEM analysis showed lattice fringes with an interplanar spacing (*d*) of 0.2602 nm corresponding to the (002) plane of hexagonal wurtzite ZnO [43], confirming the material's crystallinity. These results are consistent with those from XRD, FT-IR, and SEM-EDX analyses, verifying successful synthesis of the ZnO nanostructures.

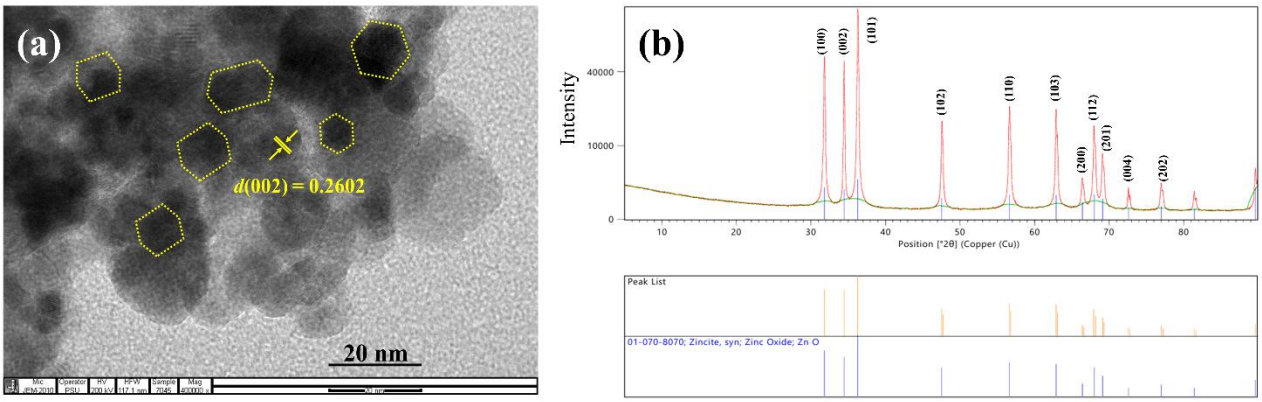


**Figure 4** Structural and crystallographic characterization of ZnO nanoparticles; (a) TEM image of synthesized ZnO NPs and (b) XRD patterns of synthesized ZnO NPs.

**XRD analysis**

The phase structures of the ZnO NPs were examined by using the powder X-ray technique (**Figure 4(b)**). The XRD pattern of the ZnO NPs correlated well with the corresponding reference hexagonal ZnO wurtzite phase (01-070-8070, Zincite, ZnO) [44]. The characteristic diffraction peaks at 2θ = 31.79°, 66.45°, 67.93°, 69.18°, 72.59°, 34.43°, 36.29° and 77.06° indicated the reflection from (100), (002), (101), (102), (110), (103), (200), (112), (201), (004) and (202) crystal planes, respectively. The average crystallite size of the synthesized ZnO NPs can be calculated from the full width at half maximum (FWHM) using the Debye-Scherrer formula [45]. The average crystallite sizes (D) of the ZnO nanostructures were calculated using Eq. (2). The crystallite sizes of 30.9 ± 4.6 nm were obtained.

$$D = 0.94\lambda/\beta\text{Cos }\theta \quad (2)$$

where D is crystallite size (nm), λ is wavelength of the X-ray source, β is broadening of diffraction line at full width half maximum (FWHM) and θ is the position of the peak.

**Table 1** Miller indices (hkl), full width half maxima of peaks (FWHM), Bragg's angle (2θ) and crystallite size using Debye-Scherrer equation for nanocrystalline ZnO.

| hkl | 2θ | FWHM (°2θ) | Crystallite size (nm) |
|---|---|---|---|
| (100) | 31.78 | 0.2814 | 29.35 |
| (002) | 34.42 | 0.2603 | 36.11 |
| (101) | 36.28 | 0.3070 | 27.23 |

The structural parameters of nanocrystalline ZnO obtained from X-ray diffraction analysis are summarized in **Table 1**. The prominent diffraction peaks guided to the (100), (002), and (101) planes confirm the hexagonal wurtzite crystal structure of ZnO [46]. The diffraction peaks at 2θ = 31.78°, 34.42° and 36.28° correspond well to the standard positions for the (100), (002), and (101) planes of hexagonal wurtzite ZnO, confirming good crystallinity and phase purity. The full width at half maximum (FWHM) values of these peaks ranged from 0.2603° to 0.3070°, indicative of peak broadening due to nanoscale crystallite size. Using the Debye-Scherrer equation, the average crystallite sizes were calculated as 29.35 nm for the (100) plane, 36.11 nm for the (002) plane, and 27.23 nm for the (101) plane. The difference in crystallite size between different planes suggests that the crystals grew in an anisotropic way. The (002) direction has a relatively larger crystallite size, which is often linked to preferential growth along the c-axis of ZnO nanocrystals [47]. The average crystallite sizes of 30 ± 4.6 nm were obtained.

**FTIR spectroscopic analysis**

The Fourier Transform Infrared (FTIR) spectra of *T. catappa* leaf extract and the green synthesized ZnO NPs was presented in **Figure 5**. The FTIR spectrum of the crude extract exhibited the broad band at 3,431 $cm^{-1}$ corresponds to O-H stretching of polyphenols group [48]. The peaks 2,922 and 2,852 $cm^{-1}$ are ascribed to asymmetric and symmetric stretching vibrations of C-H groups from aliphatic chains [49]. A strong band at 1,724 $cm^{-1}$ is assigned to the stretching vibration of carbonyl (C=O) groups, which may arise from aldehydes, ketones, or carboxylic acids [50]. The absorption at 1,618 $cm^{-1}$ corresponds to C=C stretching in aromatic rings, while the band at 1,051 $cm^{-1}$ is associated with C-O stretching vibrations, suggesting the presence of polyphenols, flavonoids, and other phytochemical constituents. The absorption band related to ZnO NPs is presented in the range of 400 to 600 $cm^{-1}$ which is shown with yellow region. This peak is assigned to Zn-O stretching vibration of hexagonal ZnO [51]. FTIR analysis of of green synthesized ZnO NPs revealed characteristic bands of plant-derived biomolecules responsible for reduction and stabilization, including 1,000 - 1,600 $cm^{-1}$ (C-O, C=C) and 2,300 - 3,500 $cm^{-1}$ (O-H, C-H), confirming successful capping by natural agents and potential biomedical applications [52].

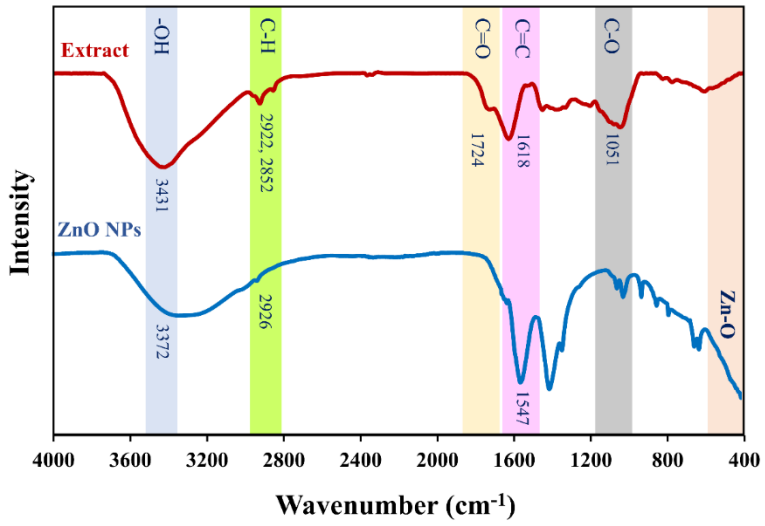


**Figure 5** FTIR spectrum of *T. catappa* leaf extract and the green synthesized ZnO NPs.

**Antifungal activity of bio-coating against *Phytophthora***

The antifungal efficiency of the bio-based coating formulations was evaluated using the agar diffusion method, with inhibition zones shown in **Figure 6**. The control exhibited an inhibition zone of 8.23 ± 0.16 cm, indicating full growth of *Phytophthora mycelium*. Whereas the bio-coating formulations showed concentration-dependent inhibition, with the ZnO NP-containing coatings showing progressively smaller zones as ZnO NP concentration increased, reaching (1.02 ± 0.06 cm) at 8% (w/w). Fungal colony growth in Petri dishes under different treatments is depicted in **Figure 6(a)**. The control plate (PDA without ZnO NPs) exhibited dense and uniform mycelium growth covering the entire surface. This result indicates that the absence of antifungal inhibition zone surrounding the inoculum, confirming their ability to suppress fungal growth. At lower concentrations (3% (w/w) and 5% (w/w)), ZnO NPs produced a distinct inhibition zone with limited mycelium development around the disc, showing moderate an antifungal activity. As the ZnO NPs concentration increased to 7% (w/w) and 8% (w/w), the inhibition zone became more obvious, and the fungal growth and the smallest visible colony diameter decreased [53]. **Figure 6(b)** presented the average mycelial diameter and the corresponding inhibition percentage. The control sample exhibited a maximum mycelial diameter of 8.23 ± 0.16 cm, representing not inhibited fungal growth. Upon addition of ZnO NPs, the mycelial diameter sharply decreased to 1.52 ± 0.11, 1.36 ± 0.08 and 1.09 ± 0.09 cm at 3% (w/w), 5% (w/w) and

7% (w/w) respectively. The growth was completely suppressed at 8%w/w and 9%w/w. Correspondingly, the inhibition percentage increased dramatically with ZnO NPs concentration, reaching nearly 100% inhibition at ≥ 8% (w/w). These results displayed a concentration-dependent antifungal activity of ZnO NPs. The higher ZnO NP concentrations led to stronger inhibition of *Phytophthora* because of the increased release of $Zn^{2+}$ ions and reactive oxygen species (ROS) that disrupt fungal cell membranes, inhibit enzyme function, and ultimately suppress mycelial proliferation. Therefore, ZnO NPs are recognized as having promising potential as an effective antifungal agent against plant pathogenic fungi.

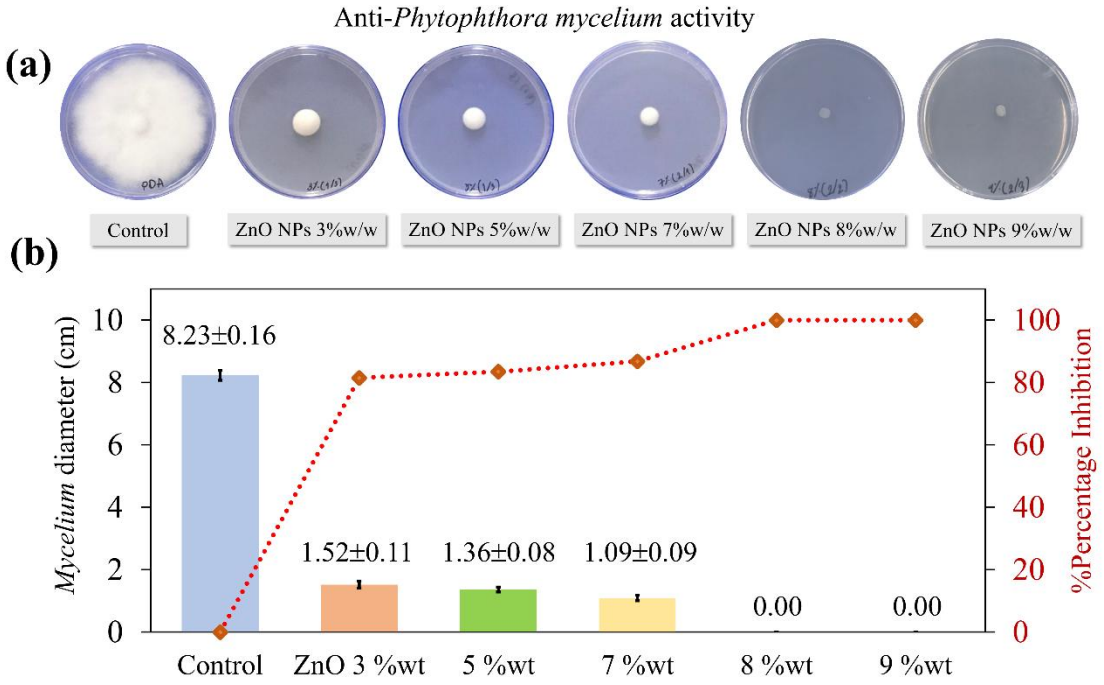


**Figure 6** Antifungal activity of bio-coating against *Phytophthora mycelium*; (a) Mycelial growth on PDA with varying ZnO NP concentrations (0% (w/w) - 9% (w/w)) (b) Mycelium diameter and percentage inhibition as a function of ZnO NP concentration.

**Study of the durian peel morphology**

The findings of the study indicated that an 8% (w/w) coating, composed of zinc oxide and chitosan, can suppress the growth of *Phytophthora* fungus. Consequently, an 8% (w/w) coating was directed to durian peels to investigate its efficiency in postponing the ripening process of durians. **Figure 7(a)** illustrates the uncoated durian peel at a magnification of 100×. The surface exhibited irregular flake-like and porous structures with rough textures. At a magnification of 500×, **Figure 7(b)** elucidates the microstructure of the uncoated peel. The fibrous network and open cavities are more distinct, illustrating the microfibril bundles and voids intrinsic to the cellulose-hemicellulose matrix. On the other hand, **Figure 7(c)** demonstrated the surface subsequent to the application of the ZnO NPs/CS composite at an equivalent magnification. The coated surface exhibits enhanced smoothness and compactness, suggesting that the ZnO NPs/CS layer effectively concealed the natural holes and imperfections of the durian peel substrate. This modification signifies the successful deposition of the composite layer, likely enhancing the barrier of material and antibacterial properties [54]. These characteristics result in elevated surface roughness while also signifying insufficient protective coating. **Figure 7(d)**, obtained at 1k× magnification, clearly shows the distribution of ZnO NPs, which appear as bright, granular spots that are uniformly embedded in and adhered to the surface, confirming a strong interfacial interaction between the ZnO NPs and the biopolymer matrix.

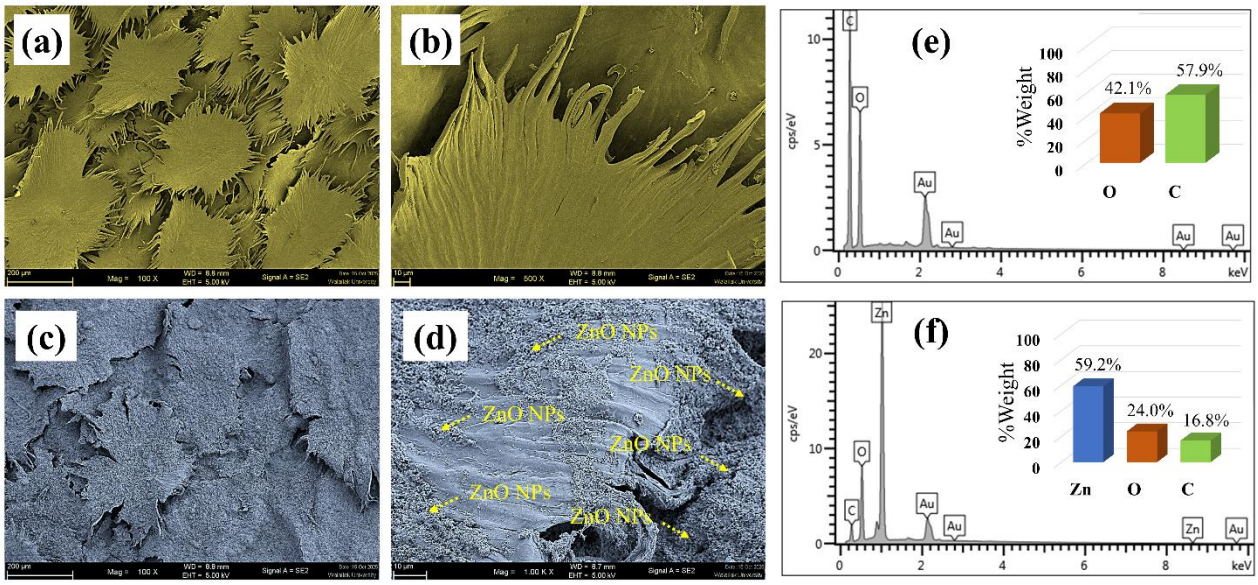


**Figure 7** SEM image of durian peel; (a) uncoated at 100×, (b) uncoated at 1k× magnification, (c) coated durian peel at 100×, (d) coated at 1k× magnification (e) EDX spectrum and %wt of element of uncoated durian peel and (f) EDX spectrum and %wt of elements of coated durian peel.

The total sugar content of coated and uncoated durian peel during storage is summarized in **Table 2**, which clearly shows the comparative sugar content. On Day 0, there were no significant changes in total sugar concentration between treatments ($p > 0.05$), which means that the samples were all about the same level of maturity before being stored. Starting on Day 3, there were significant differences in the total sugar concentration across treatments ($p < 0.05$). The uncoated control exhibited the highest increase in total sugar content throughout the storage period, reaching 23.95 ± 0.27 g/100 g by Day 10. In contrast, all coated samples showed significantly lower sugar contents compared to the control at corresponding storage times ($p < 0.05$), demonstrating the effectiveness of the coatings in delaying ripening. Among the coated treatments, the uncoated sample exhibited the strongest retardation effect on sugar accumulation, with total sugar content limited to 17.79 ± 0.48 g/100 g at Day 10, followed by the beeswax-coated (20.96 ± 0.58 g/100 g) and ZnO-coated samples (21.67 ± 0.40 g/100 g). The uncoated treatment showed significantly lower sugar levels than the beeswax- and ZnO NPs/CS coated samples at Days 3, 6, and 10 ($p < 0.05$). The superior performance of the ZnO NP/CS coating can be attributed to its enhanced barrier properties, which reduced oxygen diffusion and respiration rates, thereby slowing carbohydrate metabolism and starch-to-sugar conversion [55,56]. Additionally, incorporating ZnO NPs into the chitosan matrix likely improved film integrity and gas selectivity, further suppressing ripening-associated metabolic activity [54]. Beeswax-coated and uncoated durian exhibited moderate inhibition of sugar accumulation, indicating partial barrier effects, whereas the uncoated control showed rapid sugar increases due to unrestricted gas exchange and accelerated ripening. These findings demonstrate that the ZnO NP/CS coating outperforms conventional coatings in controlling sugar metabolism during storage, highlighting its potential for extending postharvest shelf life.

The improved barrier performance of the ZnO NP/CS coating is attributed to intermolecular interactions between chitosan chains and ZnO nanoparticles. Hydrogen bonding and water adsorption on ZnO surfaces promote a denser composite structure and increase diffusion tortuosity, thereby reducing moisture and gas transport through the coating. Fundamental studies show that water adsorption on oxide surfaces depends on electronic structure and surface defects, which influence hydrophilicity and moisture transport behavior [57-59]. These mechanisms likely contribute to the reduced weight loss and delayed sugar accumulation observed in coated durians.

**Table 2** Statistical comparison of total sugar content in coated and uncoated durian peel during storage.

| Treatment | Total Sugar g/100g | | | |
|---|---|---|---|---|
| | Day 0 (Initial) | Day 3 | Day 6 | Day 10 |
| Uncoated (Control) | $10.76 \pm 0.43^{a}$ | $15.34 \pm 0.33^{a}$ | $17.83 \pm 0.18^{a}$ | $23.95 \pm 0.27^{a}$ |
| Beeswax-coated | $10.84 \pm 0.59^{a}$ | $14.82 \pm 0.16^{b}$ | $17.22 \pm 0.45^{a}$ | $20.96 \pm 0.58^{b}$ |
| ZnO-coated | $10.82 \pm 0.53^{a}$ | $13.55 \pm 0.39^{c}$ | $16.78 \pm 0.25^{b}$ | $21.67 \pm 0.40^{b}$ |
| Blank-coated | $10.68 \pm 0.44^{a}$ | $12.18 \pm 0.24^{d}$ | $14.78 \pm 0.35^{c}$ | $17.79 \pm 0.48^{c}$ |

Note: Values are expressed as mean ± standard deviation (n = 3). Different letters within the same storage time indicate statistically significant differences among treatments according to Tukey's honestly significant difference (HSD) test ($p < 0.05$).

**Durian peel color determination**

The **Table 3** exhibited the changes of color parameters (L*, a*, b*) and total color difference (ΔE) of durian peel during storage. At Day 0, the peel exhibited high lightness (L*), strong greenness (negative a*), and moderate yellowness (b*), indicating a fresh and unripe appearance. A significant decrease in L* values was observed ($p < 0.05$), indicating gradual darkening of the peel surface. The values of a* increased from −6.42 ± 0.15 to −2.76 ± 0.32, reflecting a loss of green coloration, while b* values increased markedly from 32.18 ± 0.18 to 40.12 ± 0.38. This result indicates enhanced yellowness. Therefore, the color changes are characteristic of durian ripening and senescence. The total color difference (ΔE) increased significantly with storage time, reaching 8.24 ± 0.17 at Day 10. The progressive increase in ΔE confirms substantial visual deterioration of the durian peel during storage. These color changes are associated with chlorophyll degradation and carotenoid accumulation, processes that are closely regulated by ethylene production and respiration activity during ripening [60,61]. Increased metabolic activity accelerates pigment transformation, leading to reduced greenness, increased yellowness, and overall peel darkening.

**Table 3** Statistical analysis of peel color parameters (L, a, b*, and ΔE) of durian during storage.

| Day | L* (Lightness) | a* (Redness-Greenness) | b* (Yellowness-Blueness) | ΔE (Total Color Difference) | Observation |
|---|---|---|---|---|---|
| 0 | $69.85 \pm 0.21^{a}$ | $-6.42 \pm 0.15^{a}$ | $32.18 \pm 0.18^{a}$ | - | Fresh green peel |
| 3 | $68.91 \pm 0.34^{ab}$ | $-5.87 \pm 0.19^{ab}$ | $33.42 \pm 0.24^{ab}$ | $1.48 \pm 0.05^{a}$ | Slight color change |
| 6 | $67.43 \pm 0.33^{c}$ | $-4.28 \pm 0.25^{c}$ | $36.55 \pm 0.31^{c}$ | $4.62 \pm 0.12^{c}$ | Moderate yellowing |
| 10 | $64.87 \pm 0.42^{e}$ | $-2.76 \pm 0.32^{e}$ | $40.12 \pm 0.38^{e}$ | $8.24 \pm 0.17^{e}$ | Approaching full ripeness |

*Significant difference between days ($p < 0.05$)

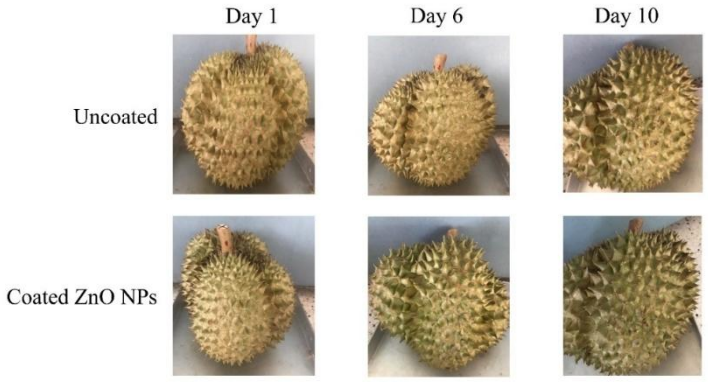


**Figure 8** Images of durian peel color changes in ZnO NPs coated durian peel compared with uncoated during storage.

**Figure 8** exhibited the visual appearance of uncoated and ZnO NPs coated durian during storage at Days 1, 6, and 10. The uncoated fruit exhibited pronounced visual changes with storage time, including peel darkening and increased yellow-brown coloration, particularly evident at day 10. These observations are consistent with the instrumental color measurements, which showed a significant decrease in L* (lightness), a loss of greenness (increase in a*), and a marked increase in b* (yellowness), resulting in a high total color difference (ΔE). In contrast, the ZnO NPs coated durian maintained a comparatively greener and lighter peel appearance throughout storage. The slower visual deterioration corresponds well with the lower ΔE values and delayed color transitions observed in the coated samples, indicating reduced chlorophyll degradation and slower pigment transformation.

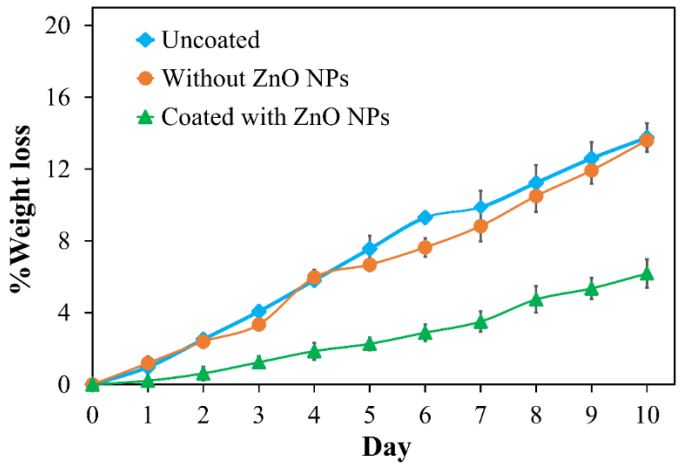


**Figure 9** Effect of chitosan and chitosan composite coatings on weight loss (%) of durian fruit during storage.

**Weight loss analysis**

In the post-harvest period, durian continues to exhibit physiological activity, particularly respiration and transpiration, resulting in continuous weight loss. This weight change is directly related to the degree of ripeness and the quality of the durian flesh [62]. Therefore, studying the percentage of weight loss is an intriguing approach for developing a quantitatively and accurately measurable indicator of ripeness. The percentage weight loss of uncoated durian peel, coated without ZnO NPs/CS, and coated with ZnO NPs/CS during storage at room temperature is shown in **Figure 9**. %Weight loss increased progressively in all treatments as storage time advanced, which is typical of postharvest water loss caused by transpiration and respiration. The uncoated durian exhibited the highest weight loss throughout the storage period, reaching 13.76 ± 0.79% by day 10. A comparable trend, although slightly reduced, was observed in the durian coated without ZnO NPs/CS. In contrast, coated durian peel showed a significantly lower rate of weight loss, remaining below 6.19 ± 0.39% at day 10. The reduced weight loss of durian peel coated ZnO NPs/CS improved mechanical strength, restricted moisture permeation, and acted as gas barriers, reducing oxidative damage and water transmission in durian coating [63]. The lower transpiration rate also contributes to delayed ripening and improved retention of visual quality, consistent with the reduced peel color changes (lower ΔE) and slower sugar accumulation observed in coated durian peel. The results demonstrated that ZnO NPs/CS based coatings effectively suppress postharvest weight loss by modulating mass transfer and respiration processes, which play a crucial role in extending the storage life and maintaining the quality of durian.

**Zn metal residues analysis**

Atomic absorption spectrometry (AAS) was used to quantify Zn residues in the durian outer peel, inner peel, and pulp of uncoated controls and ZnO NP-coated samples after 10 days of storage (**Table 4**). No Zn was detected in the pulp across all treatments or in the peels of uncoated samples. Coated samples showed only trace Zn levels (0.08 ± 0.002 mg/kg) in the inner peel,

confirming confinement of ZnO NPs to the outer coating layer with no migration into the edible pulp. This surface retention ensures food safety, as Zn remains external to internal tissues.

**Table 4** Atomic absorption spectrometry (AAS) analysis of Zn residues in durian peel (outer/inner) and pulp: uncoated controls vs. ZnO NPs/CS-coated samples after 10-day storage.

| Sample | Zn in durian inner peel (mg/kg) | Zn in durian pulp (mg/kg) |
|---|---|---|
| Uncoated | ND  | ND  |
| Without ZnO NPs/CS | ND  | ND  |
| ZnO NPs/CS composite | 0.08 ± 0.002  | ND  |

Beyond postharvest preservation, ZnO NPs/CS coatings offer broader agricultural applications, including reported antimicrobial activity, photoprotective effects, and lower toxicity compared to synthetic preservatives. Incorporating them into biodegradable biopolymers such as chitosan-alginate enables sustainable packaging that reduces food loss during transport and storage. Economically, extended shelf life minimizes postharvest losses, enhances export reliability, and optimizes supply chains for high-value climacteric fruits like durian. Future research should assess long-term environmental fate, coating biodegradability, and large-scale cost-effectiveness to facilitate commercial adoption.

**Table 5** Comparison of ZnO NPs/CS coating performance (weight loss, ripening delay) with recent biopolymer and nanocomposite coatings for postharvest shelf-life extension in horticultural commodities.

| Samples | Coating Material | Storage Conditions | Shelf-Life Extension | Referents |
|---|---|---|---|---|
| Mango | Alginate/ZnO NPs coating | Cold storage + shelf-life simulation | Shelf life extended up to 21 days | Hmmam *et al.* [64] |
| Strawberry | Chitosan + ZnO NPs with plant extracts | 4 °C and ambient conditions | Shelf life extended up to 30 days under refrigeration | Sani *et al.* [65] |
| Tomato | Chitosan-Aloe vera gel nanoemulsion + ZnO NPs | 20 °C storage | Shelf life extended to ~20 days | Iqbal *et al.* [66] |
| papaya | chitosan-based zinc oxide and silver nanoparticles coating | 14 ± 1.6 °C storage | Shelf life extended to 8 to 9 days compared to untreated fruits | Timilsina *et al.* [67] |
| Cucumber | Moringa oil-beeswax coating | 4 - 22 °C storage | Improved shelf stability during storage | Al-Rashdi *et al.* [68] |
| Durian peel (Monthong) | Chitosan + ZnO NPs | Ambient storage, | Shelf life extended to 10 days compared to untreated fruits | This study |

**Table 5** compares the ZnO NPs/CS coating developed here with recent postharvest coatings for various horticultural commodities. ZnO nanocomposite coatings consistently reduce weight loss, decay, and ripening rates across fruits. For Monthong durian under ambient storage, our ZnO NPs/CS coating achieved less

than 6.19% weight loss and delayed total soluble sugar accumulation to 21.67 g/100 g at day 10 outcomes comparable to or exceeding those for mango (e.g., 5% - 8% loss reduction), strawberry (delayed decay by 7 - 10 days), tomato (extended shelf life by 4 - 6 days), and plum (slower firmness loss) using biopolymer or ZnO-based coatings under ambient or refrigerated conditions. This underscores how ZnO incorporation enhances coating barrier properties, antimicrobial activity, and ripening control, offering a versatile strategy for extending shelf life in climacteric fruits like durian.

## Conclusions

This study demonstrates that chitosan-alginate bio-coatings incorporating green-synthesized ZnO NPs effectively delayed postharvest ripening and quality deterioration in Monthong durian. The coatings significantly reduced weight loss (< 6.19% at day 10), slowed total soluble sugar accumulation (21.67 g/100 g at day 10), and retarded peel color changes associated with chlorophyll degradation and carotenoid accumulation. These effects arise from suppressed respiration, transpiration, and starch-to-sugar conversion, facilitated by a semi-permeable barrier on the fruit peel. Notably, atomic absorption spectrometry detected no Zn in the edible pulp and only trace levels (0.08 mg/kg) in the inner peel, confirming confinement of ZnO NPs to the coating layer with no migration into edible tissues and thus validating their food safety. Overall, this sustainable approach extends durian shelf life while ensuring safety of the edible portion, offering substantial potential for postharvest management and export of climacteric tropical fruits.

## Acknowledgements

This research was funded by Nakhon Si Thammarat Rajabhat University, the Ministry of Higher Education, Science, Research and Innovation (grant numbers: NSTRU 005/2565). The authors are grateful for the equipment support offered by the Center of Excellence in Nanomaterials Chemistry, Nakhon Si Thammarat Rajabhat University, Thailand.

## Declaration of generative AI in scientific writing

The authors acknowledge the use of generative AI tools (QuillBot and ChatGPT 5.2 version by OpenAI) in the preparation of this manuscript, specifically for language editing and grammar correction. No content generation or data interpretation was performed by AI. The authors take full responsibility for the content and conclusions of this work.

## CRediT author statement

**Paweena Porrawatkul**: Conceptualization, Methodology, Supervision, Validation, Software, Funding acquisition, Writing - Original Draft and Writing-review & editing. **Prawit Nuengmatcha**: Formal analysis, Writing - Review & Editing. **Rungnapa Pimsen**: Data curation, Formal analysis. **Arnannit Kuyyogsuy**: Formal analysis, Validation. **Benjawan Ninwong**: Investigation, Validation. **Montakarn Thongsom**: Methodology, Formal analysis (Experiment and analysis of antifungal activity). **Nichapa Rattanagomon**: Resources, Investigation.

## References

[1] B Wiangsamut and MEL Wiangsamut. Assessment of natural fruit ripening and fruit quality of three elite durian cultivars for overland export. *Trends in Sciences* 2023; **20(5)**, 4647.

[2] X Y Tan, A Misran, LDJ Daim, P Ding and MSP Dek. Effect of freezing on minimally processed durian for long term storage. *Scientia Horticulturae* 2020; **264**, 109170.

[3] CL Nkwocha, AA Tsige, B Maphosa, C Coetzee and UL Opara. Optimising refrigerated container cooling performance: A virtual modelling approach for temperature and quality management in fresh fruit cold chain. *Biosystems Engineering* 2026; **262**, 104357.

[4] J Wattanasan, N Laohakunjit, N Kaisangsri, A Uthairatanakij, P Vongsawasdi and W Mingvanish. Ripeness and quality of harvested durian determined using Raman spectroscopy combined with physico-chemical and volatile characteristics. *Postharvest Biology and Technology* 2024; **213**, 112970.

[5] E Sospeter, P Ding, TH Fang, A Misran, F Abas and G Dey. Understanding the complex aroma profile of durian fruit: Aconcise review. *Journal of Food Science* 2025; **90**, e70099.

[6] J Yu, Y Tseng, K Pham, M Liu and DM Beckles. Starch and sugars as determinants of postharvest shelf life and quality: Some new and surprising

roles. *Current Opinion in Biotechnology* 2022; **78**, 102844.

[7] CY Wright, T Kapwata, S Kunene, N Kwatala, N Mahlangeni, T Laban and C Webster. Heat in the transport sector: Measured heat exposure and interventions to address heat-related health impacts in the minibus taxi industry in South Africa. *International Journal of Biometeorology* 2025; **69**, 2475-2487.

[8] RO Hernandez, AO Rocha, C Cai, M Erasmus, JS Johnson and LF Brito. Effects of microclimate during transport on physiological indicators of market pig welfare: A systematic review with meta-analysis. *Frontiers in Veterinary Science* 2025; **7(12)**, 1657185.

[9] TT Alemu, P Intipunya and BA Gebeyo. A comprehensive review of edible coatings for postharvest management of fruits and vegetables: enhancing food and nutrition security. *Discover Agriculture* 2025; **3**, 190.

[10] DA Barus, S Humaidi, RT Ginting and J Sitepu. Enhanced adsorption performance of chitosan/cellulose nanofiber isolated from durian peel waste/graphene oxide nanocomposite hydrogels. *Environmental Nanotechnology Monitoring & Management* 2022; **17**, 100650.

[11] HS Abu-Shama, FO Abou-Zaid and EZ El-Sayed. Effect of using edible coatings on fruit quality of Barhi date cultivar *Scientia Horticulturae* 2020, **265**, 109262.

[12] EM Shapiro. Biodegradable, polymer encapsulated, metal oxide particles for MRI-based cell tracking. *Magnetic Resonance in Medicine* 2015; **73(1)**, 376-389.

[13] O Olawore, M Ogunmola and S Desai. Engineered nanomaterial coatings for food packaging: Design, manufacturing, regulatory, and sustainability implications. *Micromachines* 2024; **15**, 245.

[14] A Karnwal, G Kumar, R Singh, M Selvaraj, T Malik, AR Mohammad and A Tawaha. Natural biopolymers in edible coatings: Applications in food preservation. *Food Chemistry* 2025; **25**, 102171.

[15] N Kuruthukulangara and IV Asharani. Biosynthesized MgO NPs and their environmental applications - a short review. *Journal of Cluster Science* 2024; **35**, 2681-2703.

[16] MAS Alothoum. A review of the synthesis, structural, and optical properties of $TiO_2$ nanoparticles: Current state of the art and potential applications. *Crystals* 2025; **15**, 944.

[17] X Liu, Z Xia, Y Wang, D Luo, Z Li, Z Meng and H Lian. Zinc-doped inorganic bioactive materials: A comprehensive review of properties and their applications in osteogenesis, antibacterial, and hemostasis. *Applied Materials Today* 2024; **40**, 102393.

[18] KE Mosquera-Murillo, AM Castañeda-Manquillo, KL Ángel-Camilo, PA Arciniegas-Grijalba, MM Ramírez de Valdenebro, LP Mosquera-Sanchez, IA Meza-Cabrera and JE Rodriguez-Paez. Evaluation of the toxicity of ZnO nanoparticles obtained by a chemical route on the nasal respiratory epithelium of the biomodel *Mus musculus*. *Journal of Nanoparticle Research* 2023; **25**, 258.

[19] N Babayevska, L Przysiecka, G Nowaczyk, M Jarek, M Järvekülg, T Kangur, E Janiszewska, S Jurga and I Iatsunskyi. Fabrication of gelatin-ZnO nanofibers for antibacterial applications. *Materials* 2021; **14**, 103.

[20] SZ Iqbal, M Waseem, KM Zia, M Iqbal, OA Mohammed, N Amina, G Cui, AS Doghish, MA Abdel-Reheimand and AM Khaneghah. Application of chitosan, zinc oxide nanoparticles, and Aloe vera gel edible coating for the extension in shelf life of tomatoes. *Food Packaging and Shelf Life* 2025; **50**, 101570,

[21] IG Wenten, K Khoiruddin, AK Wardani, PTP Aryanti, DI Astuti and AAIAS Komaladewi. Preparation of antifouling polypropylene/ZnO composite hollow fiber membrane by dip-coating method for peat water treatment, *Journal of Water Process Engineering* 2020; **34**, 101158.

[22] I Hmmam, MAS Ali and A Abdellatif. Alginate-based zinc oxide nanoparticles coating extends storage life and maintains quality parameters of mango fruits “cv. Kiett”. *Coatings* 2023;**13**, 362.

[23] O Boura-Theodoridou, A Giannakas, P Katapodis, H Stamatis, A Ladavos and NM Barkoula. Performance of ZnO/chitosan nanocomposite films for antimicrobial packaging applications as a function of NaOH treatment and glycerol/PVOH

blending. *Food Packaging and Shelf Life* 2020; **23**, 100456.

[24] S Sarkhel, S Kaur, R Das, A Sharma, A Kheto, D Saha and Y Kumar. Antimicrobial active packaging with biopolymers and natural extracts: Sustainable solutions and technological challenges. *Sustainable Food Technology* 2025; **4**, 1225-1261.

[25] E Shamloo, E Sadeghi, M Soltani, K Mahmoudifar, M Taghizadeh, M Arab, Z Abdi-Moghadam, A Rezagholizade-Shirvan and Shokri. Encapsulation of natural/bio-based materials as nano bio-adsorbents for removal of toxic pollutants from food products: A review. *Carbohydrate Polymer Technologies and Applications* 2025; **10**, 100870.

[26] M Ghasemlou, CJ Barrow and B Adhikari. The future of bioplastics in food packaging: An industrial perspective. *Food Packaging and Shelf Life* 2024; **43**, 101279.

[27] M Tasnim and MdN Islam. Active edible coatings for smart food preservation and sustainability: A review. *Carbohydrate Polymer Technologies and Applications* 2025; **13**, 101061.

[28] AA Sharwani, KB Narayanan, ME Khan and SS Han. Photocatalytic degradation activity of goji berry extract synthesized silver-loaded mesoporous zinc oxide (Ag@ZnO) nanocomposites under simulated solar light irradiation. *Scientific Reports* 2022; **12**, 10017.

[29] S Jafarzadeh, AM Nafchi, A Salehabadi, N Oladzad-abbasabadi and SM Jafari. Application of bio-nanocomposite films and edible coatings for extending the shelf life of fresh fruits and vegetables. *Advances in Colloid and Interface Science* 2021; **291**, 102405.

[30] BJ Arroyo, AC Bezerra, LL Oliveira, SJ Arroyo, EA de Melo and AMP Santos. Antimicrobial active edible coating of alginate and chitosan add ZnO nanoparticles applied in guavas (*Psidium guajava* L.). *Food Chemistry* 2020; **309**, 125566.

[31] LS Wahyuni, N Nuryono and AD Hatmanto. Optimizing banana preservation with bandgap-dependent curcumin-modified Cu-doped-ZnO nanoparticles in chitosan edible coatings. *Surfaces and Interfaces* 2025; **61**, 106104.

[32] B Meindrawan, NE Suyatma, AA Wardana and VY Pamela. Nanocomposite coating based on carrageenan and ZnO nanoparticles to maintain the storage quality of mango. *Food Packaging and Shelf Life* 2018; **18**, 140-146.

[33] NMD Buthelezi. Chitosan-zinc oxide nanoparticle composite coatings preserve postharvest quality of 'Rosada' cherry tomato. *HortScience* 2025; **60(4)**, 613-623.

[34] P Porrawatkul, R Pimsen, A Kuyyogsuy, P Rattanaburi and P Nuengmatcha. Morphology-dependent photocatalytic performance of ZnO nanostructures in organic dye and antibiotic degradation. *International Journal of Environmental Science and Technology* 2024; **21**, 7397-7414.

[35] AOAC International. *Official methods of analysis of AOAC International* (21st ed., Method 925.35B: Total sugars in fruit products). AOAC International, Maryland, United States, 2019.

[36] H Kaur, A Sharma, K Anand, A Panday, S Tagotra, S Kakran, AK Singh, MW Alam, S Kumar, G Bouzid, J Dalal and G Singh. Green synthesis of ZnO nanoparticles using *E. cardamomum* and zinc nitrate precursor: A dual-functional material for water purification and antibacterial applications. *RSC Advances* 2025; **15**, 16742-16765.

[37] L Zhang, Y Hu, X Wang, A Zhang, X Gao, AEGA Yagoub, H Ma and C Zhou. Ultrasound-assisted synthesis of potentially food-grade nano-zinc oxide in ionic liquids: A safe, green, efficient approach and its acoustics mechanism. *Foods* 2022; **11**, 1656.

[38] Q Zhao, L Yang, C Yao and G Chen. Ultrasonic enhanced continuous crystallization: Induction time and process control. *Industrial & Engineering Chemistry Research* 2023; **62(47)**, 20083-20095.

[39] P Sutradhar and M Saha. Synthesis of zinc oxide nanoparticles using tea leaf extract and its application for solar cell. *Bulletin of Materials Science* 2015; **38**, 653-657.

[40] CA Fernandes, NJM Nizam, SBN Krishna and VV Lakshmaiah. Biogenic synthesis of zinc oxide nanoparticles mediated by the extract of *Terminalia catappa* fruit pericarp and its

multifaceted applications. *ACS Omega* 2023; **8(42)**, 39315-39328.

[41] Pratibha, K Rajoriya, R Meena and A Kumari. Synthesis and characterisation of seeds extracts-mediated ZnO nanoparticles for antimicrobial, antioxidant and vegetative applications. *Inorganic Chemistry Communications* 2024; **167**, 112700.

[42] M Mahajan, S Kumar, J Gaur, S Kaushal, J Dalal, G Singh, M Misra and DS Ahlawat. Green synthesis of ZnO nanoparticles using *Justicia adhatoda* for photocatalytic degradation of malachite green and reduction of 4-nitrophenol. *RSC Advances* 2025; **15(4)**, 2958-2980.

[43] L Muñoz-Fernandez, LS Gomez-Villalba, O Milošević and ME Rabanal. Influence of nanoscale defects on the improvement of photocatalytic activity of Ag/ZnO. *Materials Characterization* 2022; **185**, 111718.

[44] V Jayakar, V Lokapur, BR Nityasree, RK Chalannavar, LD Lasrado and M Shantaram. Optimization and green synthesis of zinc oxide nanoparticle using Garcinia cambogia leaf and evaluation of their antioxidant and anticancer property in kidney cancer (A498) cell lines. *Biomedicine* 2021; **41**, 206-222.

[45] M Sathya, PA Shobika, M Ponnar, K Pushpanathan and S Elsi. Influence of Sr concentration on crystal structure, magnetic properties and supercapacitance performance of ZnO nanoparticles. *Journal of Materials Science: Materials in Electronics* 2022; **33**, 6745-6765.

[46] P Kumar, BK Singh, BN Pal and PC Pandey Correlation between structural, optical and magnetic properties of Mn-doped ZnO. *Applied Physics A* 2016; **122**, 740.

[47] S Baruah, RA Afre and D Pugliese. Effect of size and morphology of different ZnO nanostructures on the performance of dye-sensitized solar cells. *Energies* 2024; **17**, 2076.

[48] B Siripireddy and BK Mandal. Facile green synthesis of zinc oxide nanoparticles by *Eucalyptus globulus* and their photocatalytic and antioxidant activity. *Advanced Powder Technology* 2017; **28(3)**, 785-797.

[49] MF Hamza, Y Wei, MS Khalafalla, NS Abed, A Fouda, KZ Elwakeel, E Guibal and NA Hamad. U(VI) and Th(IV) recovery using silica beads functionalized with urea- or thiourea-based polymers-application to ore leachate. *Science of The Total Environment* 2022; **821**, 153184.

[50] KV Karthik, AV Raghu, KR Reddy, R Ravishankar, M Sangeeta, NP Shetti and ChV Reddy. Green synthesis of Cu-doped ZnO nanoparticles and its application for the photocatalytic degradation of hazardous organic pollutants. *Chemosphere* 2022; **287**, 132081.

[51] M Aliannezhadi, SZ Mirsanaee, M Jamali and FS Tehrani. The physical properties and photocatalytic activities of green synthesized ZnO nanostructures using different ginger extract concentrations. *Scientific Reports* 2024; **14(1)**, 2035.

[52] DR Jaishi, I Ojha, G Bhattarai, R Baraili, Ishwor Pathak, DR Ojha, DK Shrestha and KR Sharma. Plant-mediated synthesis of zinc oxide (ZnO) nanoparticles using *Alnus nepalensis* D. Don for biological applications. *Heliyon* 2024; **10(20)**, e39255.

[53] SHS Dananjaya, RS Kumar, M Yang, C Nikapitiya, J Lee and MD Zoysa. Synthesis, characterization of ZnO-chitosan nanocomposites and evaluation of its antifungal activity against pathogenic *Candida albicans*. *International Journal of Biological Macromolecules* 2018; **108**, 1281-1288.

[54] DJ García-García, GF Pérez-Sánchez, H Hernández-Cocoletzi, MG Sánchez-Arzubide, ML Luna-Guevara, E Rubio-Rosas, R Krishnamoorthy and C Morán-Raya. Chitosan coatings modified with nanostructured ZnO for the preservation of strawberries. *Polymers* 2023; **15**, 3772.

[55] OB Sogvar, MK Saba, A Emamifar and R Hallaj. Influence of nano-ZnO on microbial growth, bioactive content and postharvest quality of strawberries during storage. *Innovative Food Science & Emerging Technologies* 2016; **35**, 168-176.

[56] X Yan, F Meng, LP Wigati, TT Van, NTH Phuong, A Koga, F Tanaka and F Tanaka. Improvement of cross-linked films based on chitosan/diepoxy-poly (ethylene glycol) incorporating trans-cinnamaldehyde essential oil: Preparation, properties, and application in banana

storage. *International Journal of Biological Macromolecules* 2024; **263(2)**, 130299.

[57] D Nematov, K Kholmurodov, M Husenzoda, A Lyubchyk and A Burhonzoda. Molecular adsorption of $H_2O$ on $TiO_2$ and $TiO_2$: Y surfaces. *Journal of Human, Earth, and Future* 2022; **3(2)**, 213-222.

[58] AS Burhonzoda, KT Kholmurodov, AI Lyubchyk and SI Lyubchyk. A detailed comparative analysis of the structural stability and electron-phonon properties of $ZrO_2$: Mechanisms of water adsorption on t-$ZrO_2$ (101) and t-YSZ (101) surfaces. *Nanomaterials* 2023; **13(19)**, 2657.

[59] DC Perera and JC Rasaiah. Computational study of $H_2O$ adsorption, hydrolysis, and water splitting on $(ZnO)_3$ nanoclusters deposited on graphene and graphene oxides. *ACS omega* 2023; **8(35)**, 32185-32203.

[60] N Charoenchongsuk, K Ikeda, A Itai, A Oikawa and H Murayama. Comparison of the expression of chlorophyll-degradation-related genes during ripening between stay-green and yellow-pear cultivars. *Scientia Horticulturae* 2015; **181**, 89-94.

[61] Z Li, C Chen, D Zou, J Li, Y Huang, X Zheng, B Tan, J Cheng, W Wang, L Zhang, X Ye and J Feng. Ethylene accelerates grape ripening *via* increasing *VvERF75*-induced ethylene synthesis and chlorophyll degradation. *Fruit Research* 2023; **3**, 3.

[62] J Wattanasan, N Laohakunjit, N Kaisangsri, A Uthairatanakij, P ongsawasdi and W Mingvanish. Ripeness and quality of harvested durian determined using Raman spectroscopy combined with physico-chemical and volatile characteristics. *Postharvest Biology and Technology* 2024; **213**, 112970.

[63] Z Tabassum, M Girdhar, A Kumar, T Malik and A Mohan. ZnO nanoparticles-reinforced chitosan-xanthan gum blend novel film with enhanced properties and degradability for application in food packaging. *ACS Omega* 2023; **8**, 31318-31332.

[64] I Hmmam, MAS Ali and A Abdellatif. Alginate-based zinc oxide nanoparticles coating extends storage life and maintains quality parameters of mango fruits "cv. Kiett". *Coatings* 2023; **13**, 362.

[65] A Sani, D Hassan, M Ehsan, EP Sánchez-Rodríguez and DV Melo-Máximo. Improving strawberry shelf life using chitosan and zinc oxide nanoparticles from ginger-garlic extracts. *Applied Food Research* 2025; **5(1)**, 100765.

[66] SZ Iqbal, M Waseem, KM Zia, M Iqbal, OA Mohammed, N Amina, G Cui, AS Doghish, MA Abdel-Reheimand and AM Khaneghah, Application of chitosan, zinc oxide nanoparticles, and Aloe vera gel edible coating for the extension in shelf life of tomatoes. *Food Packaging and Shelf Life* 2025; **50**, 101570.

[67] S Timilsina, R Adhikari, PP Khatiwada, G Devkota and KC Dahal. Chitosan-based zinc oxide and silver nanoparticles coating on postharvest quality of papaya: Chitosan nanoparticle coating for papaya quality. *SAARC Journal of Agriculture* 2025; **22(2)**, 181-196.

[68] S Al-Rashdi, N Al-Subhi, M Al-Dairi and PB Pathare. Effect of A moringa oil-beeswax edible coating on the shelf-life and quality of fresh cucumber. *Processes* 2024; **12**, 1148.